CLINICAL AND POPULATION SCIENCES

Plaque Distribution Correlates With Morphology of Lenticulostriate Arteries in Single Subcortical Infarctions

Shuai Jiang, MD; Yuying Yan, MD; Tang Yang, MD; Qiange Zhu, MD; Changyi Wang [ID], MD; Xueling Bai, MD; Zilong Hao, MD; Shihong Zhang, MD; Qi Yang, MD; Zhaoyang Fan, PhD; Jiayu Sun, MD; Bo Wu, MD, PhD

BACKGROUND AND PURPOSE: We aimed to use novel whole-brain vessel-wall magnetic resonance imaging (WB-VWI) to investigate the association between plaque distribution of middle cerebral artery (MCA) and morphological changes of the lenticulostriate arteries (LSAs) in single subcortical infarctions.

METHODS: Forty single subcortical infarction patients with no relevant MCA disease on magnetic resonance angiography were prospectively enrolled. Plaque location in the MCA was dichotomized as proximal (located adjacent to the LSA origin) or distal (located distal to the LSA origin) on whole-brain vessel-wall magnetic resonance imaging. The MCAs with proximal plaques were divided into the symptomatic and asymptomatic side, and asymptomatic side MCAs without proximal plaques were the control group. The morphological characteristics of the LSAs and features of proximal plaques were analyzed.

RESULTS: A total of 71 MCAs in 40 patients were analyzed (31 on the symptomatic side, 22 on the asymptomatic side, and 18 in the control group). Superior-wall plaques of MCAs were observed more frequently on the symptomatic side than the asymptomatic side (45.2% versus 9.1%, $P=0.005$). The wall area index, plaque burden, and remodeling index did not differ significantly between the symptomatic and asymptomatic side. The number of LSA branches was smaller ($P=0.011$) in the symptomatic side (5.48±1.88) compared with the control group (6.83±1.92). The symptomatic side exhibited shorter average length of the LSAs (23.23±3.44 versus 25.75±3.76 mm, $P=0.025$) and shorter average distance of the LSAs (16.47±3.11 versus 21.53±4.76 mm, $P<0.001$) compared with the asymptomatic side.

CONCLUSIONS: Superiorly distributed MCA plaques at the LSA origin are closely associated with morphological changes of the LSA in symptomatic MCAs, suggesting that the distribution, rather than the inherent features of plaques, determines the occurrence of single subcortical infarctions. Our findings provide insight into the etiologic mechanism of branch atheromatous disease in single subcortical infarctions.

Key Words: brain ■ cerebral infarction ■ disease ■ magnetic resonance imaging ■ middle cerebral artery

Single subcortical infarctions (SSIs) with a nonstenotic middle cerebral artery (MCA) have been considered to be caused by lipohyalinosis and fibrinoid degeneration in small vessel disease, commonly called lacunar strokes.[1] However, large-artery atherothrombosis that blocks the orifice of the perforating artery may also be an important cause of SSIs,[2] which was termed as branch atheromatous disease (BAD) by Caplan in 1989.[3] BAD seems to be common in people of Asian origin where intracranial atherosclerosis is prevalent.[4] Although >30 years have passed since the first report, BAD remained a neglected concept.[5] Furthermore,

Nonstandard Abbreviations and Acronyms

BAD	branch atheromatous disease
ICC	intraclass correlation coefficient
LA	lumen area
LSAs	lenticulostriate arteries
MCA	middle cerebral artery
RI	remodeling index
SSIs	single subcortical infarctions
VA	vessel area
WA	wall area
WB-VWI	whole-brain vessel-wall magnetic resonance imaging

based on current stroke classification systems, physicians could misclassify a significant proportion of cases of BAD as small vessel disease or cryptogenic stroke.[6] The differentiation between BAD and intrinsic small vessel disease is of clinical importance because they might involve distinct causes, consequences, and approaches to clinical management.[7]

Over the past few decades, knowledge of the distinctions between the 2 main types of SSIs has been limited by the available imaging tools, mainly due to the lack of in vivo detection modalities with which one can directly visualize the MCA plaques and the orifice of the perforating arteries. The lenticulostriate arteries (LSAs) are the major cerebral small arteries related to SSIs and mainly supply the basal ganglia and the corona radiata.[8,9] Thus, imaging of the LSAs in vivo could enhance understanding of the differential mechanism of SSIs. However, because of the small size of perforating arteries and limited spatial-temporal resolution, visualization of LSAs in vivo remains challenging.

Recently, several studies have demonstrated that novel whole-brain vessel-wall imaging (WB-VWI) can be specifically used to visualize LSAs.[10,11] Additionally, this 3-dimensional VWI technique is capable of imaging both large-vessel wall and the LSA lumen in one image setting,[12,13] which can help further to understand the pathogenesis of SSIs. However, whether MCA plaques distribution is associated with morphological changes of the LSA in SSIs remain unknown. Recent studies using VWI reported that superior MCA wall plaques tended to be present in penetrating artery infarctions.[14,15]

According to Fisher and Caplan, the orifices of the LSAs may be blocked by focal atherosclerotic plaque of the MCA or microatheroma arising at the proximal portion of the LSA itself.[2,3] In the present study, we hypothesized that the distribution of MCA plaques is correlated with the impairment of LSAs, resulting in the occurrence of SSIs. Thus, our study aims to use WB-VWI to quantitatively evaluate the associations between distribution and characteristics of MCA plaque and morphological changes of LSAs in the symptomatic and asymptomatic sides of SSI patients and provide insight into the BAD as a nosological entity in SSIs.

METHODS

The data that support the findings of this study are available from the corresponding author upon reasonable request.

Patients

We prospectively enrolled consecutive patients who were admitted to the Department of Neurology of West China Hospital between July 2017 and December 2019 with the following inclusion criteria: (1) age 18–80 years old; (2) single subcortical infarction in the LSA territory (basal ganglia, corona radiata, and internal capsule)[16] identified using diffusion-weighted imaging performed within 7 days of symptom onset; (3) no relevant MCA disease confirmed by magnetic resonance angiography (MRA). The exclusion criteria included: (1) previous history of stroke or transient ischemic attacks on the symptomatic side; (2) coexistent ipsilateral internal carotid artery significant stenosis (≥50%) detected by computed tomographic angiography; (3) multiple lesions on diffusion-weighted imaging; (4) nonatherosclerotic vasculopathies, such as vasculitis, dissection, or Moyamoya disease; and (5) evidence of potential sources of cardioembolism (eg, atrial fibrillation, recent myocardial infarction, dilated cardiomyopathy, valvular heart disease, and infective endocarditis). All patients underwent 24 hours of electrocardiographic monitoring or Holter monitor and transthoracic echocardiography to exclude cardioembolism. All of the enrolled patients underwent WB-VWI within 2 weeks of symptom onset.

The flowchart for patient selection is shown in Figure I in the Data Supplement. Among the 47 patients who were recruited, 7 patients were excluded from statistical analysis due to poor image quality (N=3), MCA stenosis (N=2), and patients with other causes (N=2). A total of 40 patients (age range, 37–79 years; mean age, 55.6 years; 30 males) with a nonstenotic MCA (71 MCAs) were included for analysis.

Demographic data and clinical information were recorded, including sex, age, vascular risk factors (hypertension, diabetes mellitus, hyperlipidemia, cardiac arrhythmia, coronary artery disease, previous stroke history, and current smoking), and onset time of stroke were recorded for each patient. National Institutes of Health Stroke Scale score was measured at the time of admission. The median interval between symptom onset and WB-VWI was 7 days (ranging from 1 to 14 days). Patient demographics and main atherosclerosis risk factors are presented in Table 1. Informed consent was obtained from all participants, and all protocols were approved by the ethics committee of the West China Hospital.

Magnetic Resonance Imaging Protocols

Magnetic resonance imaging (MRI) was performed on 3.0-tesla systems (MAGNETOM Trio, Siemens, Erlangen, Germany) equipped with 32-channel head coil. The protocol included conventional diffusion-weighted imaging, 3-dimensional time-of-flight MRA, and WB-VWI. Imaging parameters for diffusion-weighted imaging were TR/TE of 4000/91 ms; field of view

Table 1. Demographic and Clinical Data of SSI Patients

Patient Characteristics	Value
Male, n (%)	30 (75.0)
Age, y (mean±SD)	55.60±10.11
Hypertension, n (%)	23 (57.5)
Diabetes mellitus, n (%)	15 (37.5)
Hyperlipidemia, n (%)	14 (35.0)
Current smoking, n (%)	21 (52.5)
Coronary heart disease, n (%)	1 (2.5)
NIHSS, median (IQR)	3.5 (1.25–6)
Onset to WB-VWI time, d, median (IQR)	7 (5–8)

IQR indicates interquartile range; NIHSS, National Institutes of Health Stroke Scale; SSI, single subcortical infarction; and WB-VWI, whole-brain vessel-wall magnetic resonance imaging.

220×220 mm2; 20 slices with slice thickness of 5 mm; voxel size=1.1×1.1×5 mm3; 2 b values of 0 and 1000 s/mm²; scan time of 1:53 minutes. Three-dimensional time-of-flight MRA was performed: TR/TE=22/4 ms; field of view=170×170 mm²; 176 slices with slice thickness of 0.53 mm; voxel size=0.53×0.53×0.53 mm3; and scan time=6 minutes. WB-VWI sequence was performed based on inversion-recovery prepared sampling perfection with application-optimized contrast using different flip angle evolutions[10,17] with the following parameters: TR/TE=900/14 ms; field of view=170×170 mm²; 240 slices with slice thickness of 0.53 mm; voxel size=0.53×0.53×0.53 mm³; and scan time=8 minutes.

Image Analysis

Commercial software (Osirix MD, Pixmeo SARL, Bernex, Switzerland) with 3-dimensional multiplanar reformation and region-of-interest signal measurement was used for image analysis. WB-VWI images were first evaluated by an experienced reader (Dr Jiang) who was blinded to the patient's clinical details and routine images. A second experienced neuroradiologist (Dr Sun) performed quantification for assessing interobserver agreement, and observer 1 requantified the measures 2 months after the first reading session for assessing intraobserver agreement. Ten MCAs were randomly selected to study the reproducibility of the quantitative measurements. Discrepancies between the 2 observers were solved by consensus.

Plaque Location on MCA and LSA Origin

To visualize the spatial relationship between MCA plaques and the LSA origin, multiplanar reconstruction, and coronal minimum intensity projection were constructed in one image setting with WB-VWI images. Plaque location in the MCA (M1≈M2 segment) was dichotomized as proximal (located adjacent to the LSA origin; Figure 1A) and distal (located distal to the LSA origin; Figures 1B). Only the proximal plaques were incorporated in the analysis.

The MCAs with proximal plaques were divided into the symptomatic side and the asymptomatic side based on the location of the acute infarcts. Asymptomatic side MCAs without proximal plaque were the control group. The morphological characteristics of the LSAs were evaluated in the 3 groups.

LSA Morphometry

LSA images were generated using coronal minimum intensity projection with 10 to 20 mm thickness on WB-VWI. To delineate the distributions of the LSAs, signal measurements of the LSAs were performed on the consecutive minimum intensity projection images, ensuring the vascular skeleton by manually tracing reflected the full length of the visualized LSAs. An LSA tracing continued only when the artery could be demonstrated as a continuous, linear low signal and clear contrast with surrounding tissue, and pointed toward the anterior perforated substance. The morphological characteristics of the visible LSAs were quantitatively analyzed on both the symptomatic and asymptomatic sides on the coronal slab minimum intensity projection image, including the number of stems and branches, length, distance, and tortuosity. Stems were defined as the portion of the LSAs that originated directly from the MCA. Branches are defined as daughter vessels originating from parent LSA stems or as stems with no branches (single vessel). LSA stems 5 mm or more in length were included for analysis. When an artery branched within 5 mm of the origin of the MCA, each stem was counted separately,[18] because >70% of branches were found to originate from common trunks.[19] When an artery branched at a more distal site, the stem was counted and measured using the longest branch. The LSA tortuosity was defined as the ratio of 2 measurements: the actual path length divided by the linear distance.[20] The schematic in Figure 2 illustrates the method used for counting stems and branches and for measuring LSAs.

Traditional Parameters of MCA Plaque

Bilateral MCAs with proximal plaques in the subjects were analyzed for artery wall abnormalities by longitudinal and cross-sectional views. An atherosclerotic plaque was defined as eccentric wall thickening on the reconstructed WB-VWI images using its adjacent proximal, distal, or contralateral normal vessel segment as a reference.[13] The lesion site was defined as the slice with the maximal wall thickening of MCA. The vessel area (VA) and lumen area (LA) were measured by manually tracing vessel and lumen boundaries. The difference between VA and LA was the wall area (WA; ie, WA=VA—LA). Plaque area was defined as the difference between WA at the lesion site and reference site. The plaque burden was calculated as plaque area/lesion VA×100%. The WA index was defined as the ratio of the lesion WA to the reference WA. And the remodeling index (RI) was calculated as the ratio of the lesion VA to the reference VA.

MCA Plaque Distribution

To evaluate the primary plaque distribution in an MCA, each cross-sectional image of MCA proximal plaque was reviewed. Based on the position of maximal wall thickening, the cross-sectional distribution of the plaque was divided into 4 quadrants: superior, inferior, ventral, and dorsal according to the previous report (Figure 3A and 3C).[14] A quadrant involved by plaque was defined as the plaque present along >50% of the circumference of that quadrant. Because plaque irregularity for the MCA in the cross-sections would lead to underestimation of the plaque involved quadrants, we also combined the long axis of the MCA vessels in reconstructed planes of WB-VWI
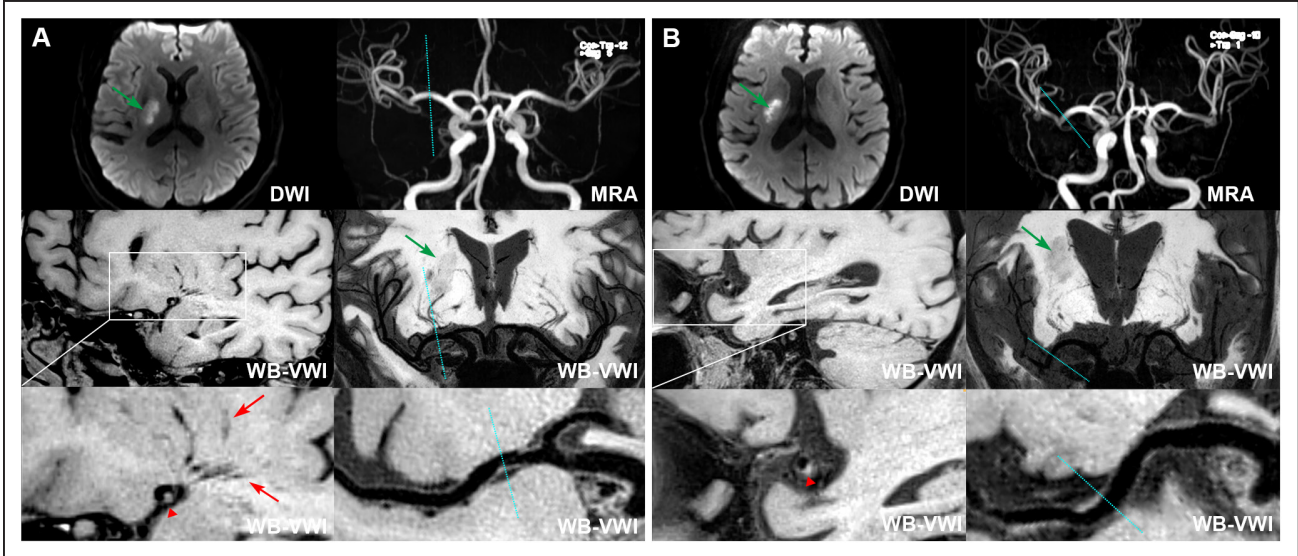
Figure 1. Classification of proximal plaque and distal plaque on middle cerebral artery (MCA).
Two representative cases of proximal plaque (located adjacent to the lenticulostriate artery [LSA] origin; (**A**) and distal plaque (located distal to the LSA origin; (**B**) on MCA. **A**, Diffusion-weighted imaging (DWI) and coronal minimum intensity projection (MinIP) showed a single subcortical infarction in the right LSA territory (green arrows); Magnetic resonance angiography (MRA) showed no stenosis on the relevant MCA; Coronal MinIP revealed shorter lengths of right LSAs compared with the left side and the curved multiplanar reconstruction (curved-MPR) showed a plaque adjacent to the corresponding LSA origins (blue dashed lines); corresponding cross-section view also demonstrated a traceable LSAs (red arrows) originating from the dorsally located plaque (arrowhead) of MCA. **B**, DWI and coronal MinIP showed a single subcortical infarction in the right LSA territory (green arrows); MRA showed no stenosis on the relevant MCA; Coronal MinIP revealed shorter lengths of right LSAs compared with the left side, but the curved-MPR showed a plaque distal to the corresponding LSA origin vessel segment of MCA (blue dashed lines); corresponding cross-section view demonstrated a dorsal plaque without traceable LSAs from the MCA wall.

images to evaluate the plaque distributions (Figure 3B and 3D). In the case of plaque that was distributed in 2 or more quadrants simultaneously, each quadrant was counted separately.

Statistical Analysis

Quantitative data are presented as means ± SD or as medians with interquartile range when the data showed a non-normal distribution, and categorical variables were summarized as count (percentage). Categorical variables were analyzed using a χ^2 test or Fisher exact test. Differences in WA index, plaque burden, and RI between symptomatic and asymptomatic MCAs were assessed using the Student t test. The LSA features (the number of stems and branches, length, distance, and tortuosity) among symptomatic side, asymptomatic side, and controls were evaluated with a 1-way ANOVA or Kruskal-Wallis test as appropriate and post hoc pairwise comparisons. Intrarater and interrater agreements of the visual assessments and measurements were determined using intraclass correlation coefficients (ICCs). Reliabilities below 0.40 were characterized as poor, 0.40 to 0.75 as fair to good, and >0.75 were considered as excellent. A P value of <0.05 indicated statistical significance. All statistical analyzes were performed by using commercial software (SPSS 25.0, IBM).
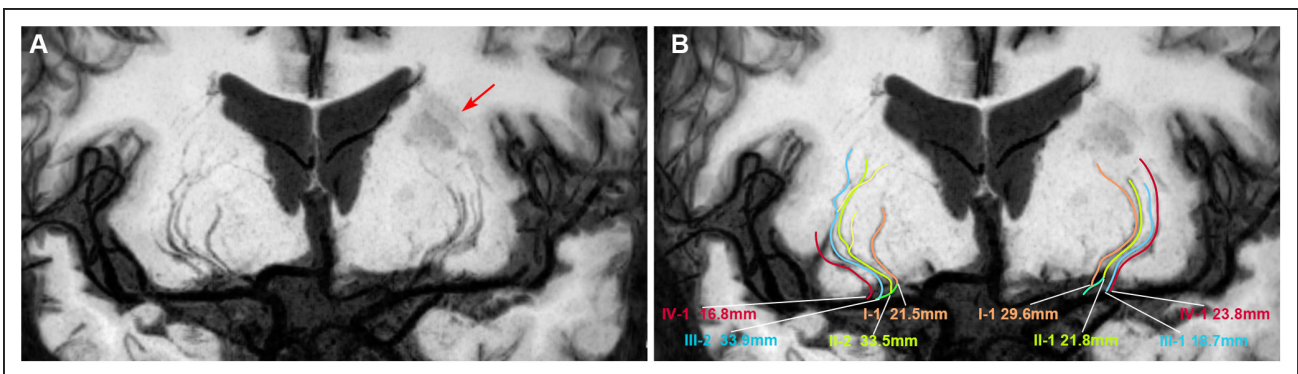
Figure 2. Methodology for measuring the lenticulostriate arteries (LSAs).
A, The reconstructed coronal minimum intensity projection (MinIP; 30 mm thickness for presentation) image of a 54-year-old female with an acute infarction in left basal ganglia (arrow). **B**, Corresponding line tracings of the LSAs. Stems are labeled with Roman numerals, whereas branches are labeled with Arabic numerals. I-1, II-2, III-2 of the right LSAs and I-1, II-1 of the left LSAs originated from the common stem. The measurements are the lengths of each stem, respectively. Compared with the asymptomatic side, smaller number of LSA branches (6 vs 4) and shorter total lengths of LSAs (105.7 vs 93.9 mm) are observed in the symptomatic side.
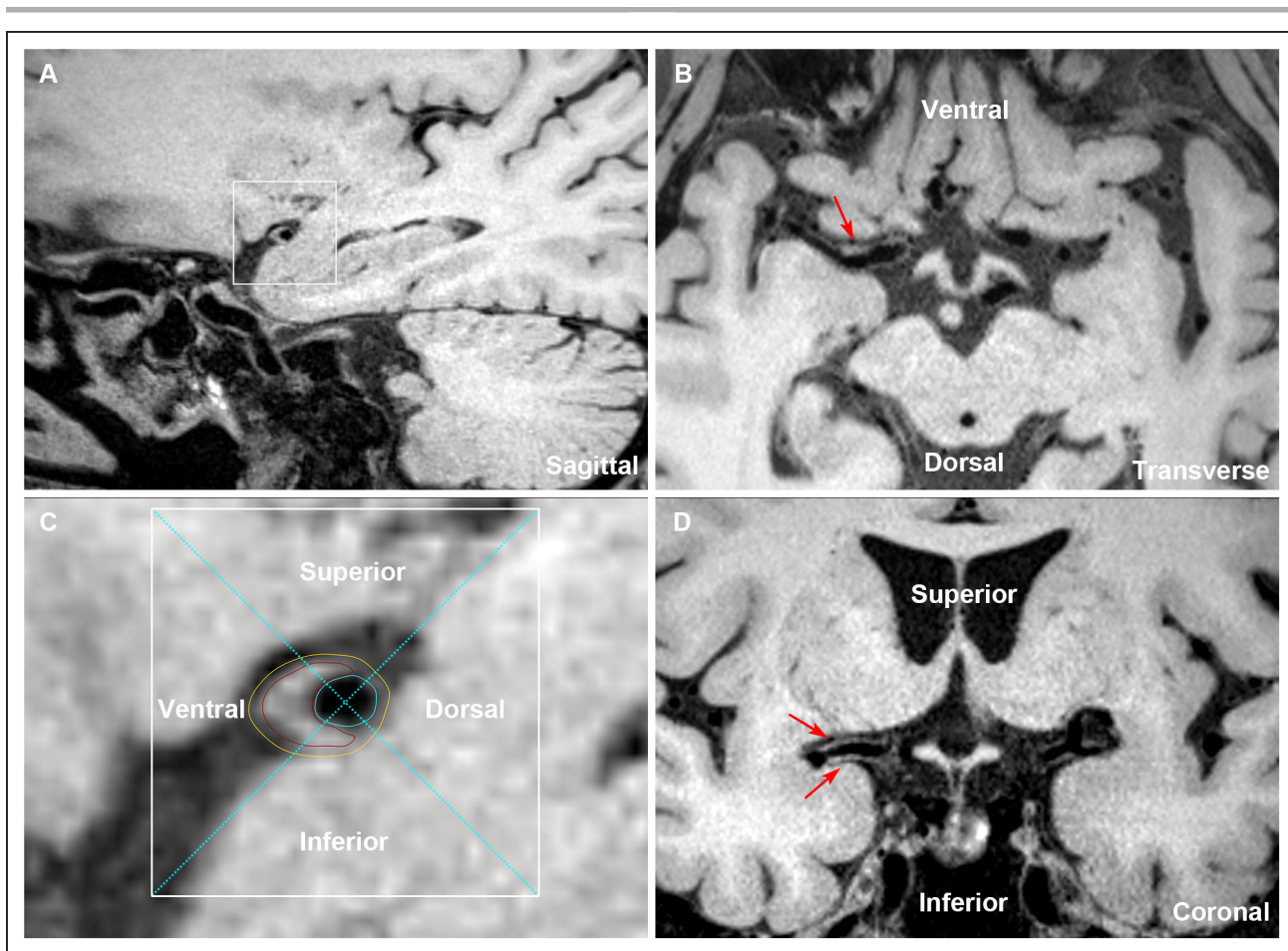
Figure 3. The plaque distribution on middle cerebral artery (MCA) walls.
A cross-section of plaque was divided into 4 quadrants (superior, inferior, ventral, and dorsal) using 2 perpendicular dashed lines that intersect at the lumen center, as shown by the enlarged image of plaque. The lumen area was outlined by blue lines, the outer wall area was outlined by yellow lines, and the estimated plaque was outlined by red lines (**A** and **C**). The reconstructed transverse and coronal views of MCA walls were used to further verify the involved quadrants of the plaque (**B** and **D**). The insets showed a typical plaque mainly involving the ventral, superior, and inferior wall (**C**, red lines; **B** and **D**, arrows).

RESULTS

Reproducibility of Quantitative Measurements

For the intraobserver agreement in assessment of plaque features, the ICC (95% CI) was 0.94 (0.78–0.98), 0.93 (0.70–0.98), and 0.92 (0.73–0.98) for WA index, plaque burden, and RI, respectively. For measuring the number of stems and branches of LSA, the intraobserver ICC was 0.95 (0.80–0.99) and 0.87 (0.56–0.97). The intraobserver ICC was 0.95 (0.81–0.99), 0.97 (0.90–0.99), and 0.99 (0.94–1.00) for measuring the average length of LSA, average distance of LSA, and average tortuosity of LSA, respectively.

For the interobserver agreement in assessment of plaque features, the ICC (95% CI) was 0.89 (0.56–0.97), 0.91 (0.62–0.98), and 0.87 (0.56–0.97) for WA index, plaque burden, and RI, respectively. For measuring the number of stems and branches of LSA, the interobserver ICC was 0.89 (0.63–0.97) and 0.85 (0.54–0.96). The interobserver ICC was 0.90 (0.59–0.98), 0.93

(0.71–0.98), and 0.98 (0.90–0.99) for measuring the average length of LSA, average distance of LSA, and average tortuosity of LSA, respectively.

MCA Plaque Distribution and LSA Origin

Of the 40 patients (totally 80 MCAs), WB-VWI detected 53 (66.3%) plaques located adjacent to LSA origin (proximal plaques) of MCAs that did not have stenosis on MRA. Proximal plaques were more frequently located on the symptomatic side 31 (77.5%) MCAs than on the asymptomatic side 22 (55.0%) MCAs (*P*=0.033).

The distribution of the proximal plaques found on the symptomatic and asymptomatic sides MCAs are shown in Table 2. Overall, proximal plaques were most commonly distributed on the ventral (71.0% versus 77.3%) and inferior (58.1% versus 68.2%) locations in both symptomatic and asymptomatic sides MCAs. Of note, the prevalence of superiorly located plaques was significantly higher in

Table 2. Plaque Distribution Between the Symptomatic Side and the Asymptomatic Side MCAs in SSI Patients

Plaque Distribution*	Symptomatic Side MCAs (n=31)	Asymptomatic Side MCAs (n=22)	P Value
Superior	14 (45.2%)	2 (9.1%)	0.005
Inferior	18 (58.1%)	15 (68.2%)	0.454
Dorsal	8 (25.8%)	2 (9.1%)	0.166
Ventral	22 (71.0%)	17 (77.3%)	0.608

MCA indicates middle cerebral artery; and SSI, single subcortical infarction.

*A plaque could involve 1–4 orientations. Therefore, the 4 orientations are independent and exceed total number of MCAs when summed up.

the symptomatic than asymptomatic sides MCAs (45.2% versus 9.1%, $P=0.005$).

MCA Plaque Characteristics and LSAs Morphological Changes

A total of 53 MCAs with proximal plaques were analyzed for plaque features, including 31 in the symptomatic side and 22 in the asymptomatic side. The WA index, plaque burden, and RI did not differ significantly between the 2 groups.

To investigate LSAs morphological changes, 18 asymptomatic side MCAs without proximal plaques were included as normal controls. There was no significant difference in the number of stems found among the symptomatic side (3.00, 7.00), asymptomatic side (4.00, 5.00), and control group (4.00, 5.00). The number of LSA branches was smaller in the symptomatic side (5.48±1.88) than in control group (6.83±1.92; $P=0.011$), whereas no significant difference was found between the symptomatic side and asymptomatic side (6.14±1.32; $P=0.211$), as well as the asymptomatic side versus the control group ($P=0.182$).

The symptomatic side had a shorter average length and distance of LSAs than both the asymptomatic side (23.23±3.44 versus 25.75±3.76 mm, $P=0.025$;

16.47±3.11 versus 21.53±4.76 mm, $P<0.001$, respectively) and the control group (23.23±3.44 versus 26.71±4.86 mm, $P=0.004$; 16.47±3.11 versus 21.84±3.61 mm, $P<0.001$, respectively). However, no statistically significant differences were found between the asymptomatic side and control group. The average tortuosity of the relevant LSAs also showed no significant differences between the 3 groups. Plaque features and morphological characteristics of the LSAs are described in Table 3.

DISCUSSION

In the present study, we found that MCA proximal plaques occurred more often on the ipsilateral than the contralateral side to SSIs. In addition, superior-wall proximal plaques of the MCA were observed more frequently on the symptomatic side than the asymptomatic side. Furthermore, a significant reduction in the number of LSA branches, the average length, and distance of LSAs in the symptomatic side MCAs were also found. However, we did not find significant differences of plaque characteristics between the symptomatic and asymptomatic side MCAs. These results suggest that the MCA plaque distribution, rather than the plaque inherent features, are associated with symptomatic LSAs, resulting in the occurrence of SSIs. To the best of our knowledge, this is the first study using WB-VWI to visualize the spatial relationship between MCA plaques and LSA origin, thus providing insight into the etiologic mechanism of BAD in SSIs.

LSAs are a major source of the blood supply for the basal ganglia and its adjacent brain regions, occlusion of which is closely associated with the occurrence of SSIs. Although flow-sensitive black-blood MRI can successfully delineate the LSAs,[18,21] it is still associated with inadequate suppression of cerebrospinal fluid signals,

Table 3. Plaque Features of MCAs and Morphological Characteristics of the LSAs

| | Symptomatic Side MCAs (n=31) | Asymptomatic Side MCAs (n=22) | Controls (n=18) | | P Value | | |
					Symptomatic vs Controls	Asymptomatic vs Controls	Symptomatic vs Asymptomatic
Wall area index	1.39±0.24	1.32±0.26	…	0.313	…	…	…
Plaque burden, %	19.05±9.67	15.53±10.75	…	0.219	…	…	…
Remodeling index	1.11±0.17	1.06±0.20	…	0.320	…	…	…
LSA stems* (n)	5.00 (3.00–7.00)	4.50 (4.00–5.00)	5.00 (4.00–5.00)	0.809	…	…	…
LSA branches (n)	5.48±1.88	6.14±1.32	6.83±1.92	0.036	0.011	0.211	0.182
Total length of LSAs, mm	104.67±37.15	116.75±30.51	124.87±24.50	0.101	…	…	…
Total distance of LSAs, mm	85.86±30.51	97.08±26.71	102.34±19.93	0.099	…	…	…
Average length of LSA, mm	23.23±3.44	25.75±3.76	26.71±4.86	0.008	0.004	0.446	0.025
Average distance of LSA, mm	16.47±3.11	21.53±4.76	21.84±3.61	<0.001	<0.001	0.796	<0.001
Average tortuosity of LSA	1.22±0.06	1.23±0.08	1.22±0.07	0.893	…	…	…

Except where indicated, data are mean±SD. IQR indicates interquartile range; LSA, lenticulostriate artery; and MCA, middle cerebral artery.

*Data are median (IQR).

which may be detected as the same signal void of LSAs. The WB-VWI technique offers whole-brain coverage with isotropic high-spatial resolution, and most importantly, adequately suppresses the cerebrospinal fluid and provides enhanced TI contrast weighting.[10,11] These advantages enable it to visualize LSA morphology and MCA plaque characteristics at the same time.

Several studies have shown that MCA plaques can be detected in 45.6% to 60% of patients with SSIs by 2-dimensional VWI,[15,22,23] suggesting that parent artery atherosclerotic plaques occluding the orifice of LSAs, termed as BAD, are an important cause of SSIs. In this study, we used a novel WB-VWI technique to more precisely locate MCA plaques at the origin of LSAs and found proximal plaques MCAs in 66.3% of SSI patients. Such a high prevalence of plaques in a normal-appearing MCA may be due to the novel 3-dimensional isotropic high-resolution vessel wall imaging allowing for the detection of small plaques. Conversely, the arterial lumen can remain normal at the early stages of atherosclerosis because of positive arterial remodeling defined as RI >1.05.[24] In our study, the RI of the symptomatic and asymptomatic sides proximal plaques were 1.11±0.17 and 1.06±0.20, suggesting that the great majority of MCAs showed positive remodeling, although there was no distinct difference between the 2 sides (*P*=0.320).

A previous study applying this novel technique demonstrated deep-perforator infarction had a significant reduction in length of LSAs compared with the healthy subjects.[25] However, the study only enrolled patients with distinct stenosis or irregularity on the relevant MCA or intracranial internal carotid artery, whose stroke cause could be apparently classified into large-artery atherosclerosis according to conventional imaging modalities. The present study mainly focused on SSI patients with a nonstenotic MCA which is often ignored and categorized as a homogeneous entity in clinical practice. We also found the symptomatic side had a shorter average length and distance of LSAs than both the asymptomatic side and the control group, which was in line with the previous studies.[25,26] This could be explained by proximal plaques occlusion of the LSAs, which can cause clipping or blood flow disturbance of the microvessels, decreasing imaging signal intensity, and eventually resulting in nonvisualization of the affected LSAs.[27] However, we only found the number of visible branches in the symptomatic side was substantially smaller than the control group but not the case of LSA stems. This might be due to the relatively small size of the LSA branches compared with the stems, making them susceptible to resolution limitations. Another possibility is that MCA positive remodeling plaques at the LSA origin, representative of unstable plaques,[24] may cause artery-to-artery micro-embolism occluding of the distal branches of LSAs. In addition, recanalization of occluded arteries in acute infarction can occur in embolisms to LSAs,[28] also making the number of LSA stems unchanged in symptomatic side MCAs.

Unexpectedly, however, the features of MCA plaques, including the WA index, plaque burden, and RI, were not statistically significant difference between the symptomatic and asymptomatic sides. A recent study using WB-VWI had a similar result between symptomatic and asymptomatic intracranial atherosclerotic stenosis patients.[13] Nevertheless, we observed that superiorly located plaques were significantly more commonly observed in the symptomatic side than the asymptomatic side. Microanatomy and ultra-high-field time-of-flight MRA in vivo studies have demonstrated that most of penetrating arteries arise dorsally from the upper part of MCA wall.[8,29] Moreover, superior-wall plaques on MCA have been reported to be related to penetrating artery infarcts. The strength of this study was that it provided direct evidence in vivo that MCA culprit plaques are nearer to the orifice of penetrating arteries, which strongly demonstrated that BAD should be considered as an important nosological entity of SSIs. Therefore, our results suggested that the distribution, rather than the burden, of plaques is important for impairing the relevant LSAs, and thus determining the presence of SSIs. These findings are clinically meaningful. Aggressive treatment to optimize plaque stabilization, including dual antiplatelet agents and intensive antiatherosclerotic medication, may be more appropriate for BAD patients in SSIs, even those with normal MCA by MRA. Furthermore, intracranial angioplasty stenting and angioplasty should be planned in a cautious manner to prevent snowplowing effects even in a patient with low plaque burden but superior plaque near the orifices of the MCA LSAs.

There are some limitations of this study. First, the sample size was relatively small, mainly because of the strict exclusion criteria. The asymptomatic side MCAs without proximal plaques defined as the control group may not represent a completely healthy population. Further large sample size studies, including symptomatic and asymptomatic SSI patients, are needed to fully investigate and verify this result. Second, we did not evaluate all possible features of intracranial plaque, such as intraplaque hemorrhage and plaque contrast enhancement, which may further improve the identification of culprit plaques. Third, due to the tortuous angulation and 3-dimensional space of the LSAs trajectories, manual tracing of LSAs is time consuming and subjective, although we applied the same counting rule to all participants. Advanced automatic segmentation and reconstruction of LSAs should be introduced to facilitate the image postprocessing and improve measurement accuracies. Fourth, the signal-to-noise ratio on 3T VWI may be insufficient for identifying the far end of the LSAs. Since the high signal-to-noise ratio provided by the 7T MRI was found to be superior in visualizing small perforating vessels compared with 3T MRI,[30,31] additional confirmatory studies and

reproducibility of the data analysis using 7T MRI scanners are needed to be explored in the future. Finally, longitudinal studies are warranted to investigate and expound on the role of LSA morphometry in the prediction of stroke recurrence and outcome.

In conclusion, WB-VWI is capable of investigating the spatial relationship between LSA origin and atherosclerotic MCA plaques in one image acquisition. Superiorly distributed MCA plaques at LSA origin are closely associated with morphological changes of LSA in symptomatic MCAs, suggesting that the distribution, rather than the inherent features of plaques, determines the occurrence of SSIs. This novel technique has great potential to be used for elucidation the stroke etiologic mechanism of SSIs.

ARTICLE INFORMATION

Affiliations

Departments of Neurology (S.J., Y.Y., T.Y., Q.Z., C.W., X.B., Z.H., S.Z., B.W.) and Radiology (J.S.), West China Hospital, Sichuan University, Chengdu, China. Department of Neurology, The Third People's Hospital of Chengdu, China (S.J.). Department of Radiology, Xuanwu Hospital, Capital Medical University, Beijing, China (Q.Y.). Biomedical Imaging Research Institute, Cedars Sinai Medical Center, Los Angeles, CA (Z.F.).

Acknowledgments

Sources of Funding

Disclosures

None.

REFERENCES

1. Fisher CM. Lacunes: small, deep cerebral infarcts. *Neurology*. 1965;15:774–784. doi: 10.1212/wnl.15.8.774
2. Fisher CM, Caplan LR. Basilar artery branch occlusion: a cause of pontine infarction. *Neurology*. 1971;21:900–905. doi: 10.1212/wnl.21.9.900
3. Caplan LR. Intracranial branch atheromatous disease: a neglected, understudied, and underused concept. *Neurology*. 1989;39:1246–1250. doi: 10.1212/wnl.39.9.1246
4. Gorelick PB, Wong KS, Bae HJ, Pandey DK. Large artery intracranial occlusive disease: a large worldwide burden but a relatively neglected frontier. *Stroke*. 2008;39:2396–2399. doi: 10.1161/STROKEAHA.107.505776
5. Kim JS, Yoon Y. Single subcortical infarction associated with parental arterial disease: important yet neglected sub-type of atherothrombotic stroke. *Int J Stroke*. 2013;8:197–203. doi: 10.1111/j.1747-4949.2012.00816.x
6. Ay H, Furie KL, Singhal A, Smith WS, Sorensen AG, Koroshetz WJ. An evidence-based causative classification system for acute ischemic stroke. *Ann Neurol*. 2005;58:688–697. doi: 10.1002/ana.20617
7. Nah HW, Kang DW, Kwon SU, Kim JS. Diversity of single small subcortical infarctions according to infarct location and parent artery disease: analysis of indicators for small vessel disease and atherosclerosis. *Stroke*. 2010;41:2822–2827. doi: 10.1161/STROKEAHA.110.599464
8. Umansky F, Gomes FB, Dujovny M, Diaz FG, Ausman JI, Mirchandani HG, Berman SK. The perforating branches of the middle cerebral artery. A microanatomical study. *J Neurosurg*. 1985;62:261–268. doi: 10.3171/jns.1985.62.2.0261
9. Marinkovic SV, Milisavljevic MM, Kovacevic MS, Stevic ZD. Perforating branches of the middle cerebral artery. Microanatomy and clinical significance of their intracerebral segments. *Stroke*. 1985;16:1022–1029. doi: 10.1161/01.str.16.6.1022
10. Yang Q, Deng Z, Bi X, Song SS, Schlick KH, Gonzalez NR, Li D, Fan Z. Whole-brain vessel wall MRI: a parameter tune-up solution to improve the scan efficiency of three-dimensional variable flip-angle turbo spin-echo. *J Magn Reson Imaging*. 2017;46:751–757. doi: 10.1002/jmri.25611
11. Ma SJ, Sarabi MS, Yan L, Shao X, Chen Y, Yang Q, Jann K, Toga AW, Shi Y, Wang DJJ. Characterization of lenticulostriate arteries with high resolution black-blood T1-weighted turbo spin echo with variable flip angles at 3 and 7 Tesla. *Neuroimage*. 2019;199:184–193. doi: 10.1016/j.neuroimage.2019.05.065
12. Zhang Z, Fan Z, Kong Q, Xiao J, Wu F, An J, Yang Q, Li D, Zhuo Y. Visualization of the lenticulostriate arteries at 3T using black-blood T1-weighted intracranial vessel wall imaging: comparison with 7T TOF-MRA. *Eur Radiol*. 2019;29:1452–1459. doi: 10.1007/s00330-018-5701-y
13. Wang M, Wu F, Yang Y, Miao H, Fan Z, Ji X, Li D, Guo X, Yang Q. Quantitative assessment of symptomatic intracranial atherosclerosis and lenticulostriate arteries in recent stroke patients using whole-brain high-resolution cardiovascular magnetic resonance imaging. *J Cardiovasc Magn Reson*. 2018;20:35. doi: 10.1186/s12968-018-0465-8
14. Xu WH, Li ML, Gao S, Ni J, Zhou LX, Yao M, Peng B, Feng F, Jin ZY, Cui LY. Plaque distribution of stenotic middle cerebral artery and its clinical relevance. *Stroke*. 2011;42:2957–2959. doi: 10.1161/STROKEAHA.111.618132
15. Yoon Y, Lee DH, Kang DW, Kwon SU, Kim JS. Single subcortical infarction and atherosclerotic plaques in the middle cerebral artery: high-resolution magnetic resonance imaging findings. *Stroke*. 2013;44:2462–2467. doi: 10.1161/STROKEAHA.113.001467
16. Tatu L, Moulin T, Bogousslavsky J, Duvernoy H. Arterial territories of the human brain: cerebral hemispheres. *Neurology*. 1998;50:1699–1708. doi: 10.1212/wnl.50.6.1699
17. Fan Z, Yang Q, Deng Z, Li Y, Bi X, Song S, Li D. Whole-brain intracranial vessel wall imaging at 3 Tesla using cerebrospinal fluid-attenuated T1-weighted 3D turbo spin echo. *Magn Reson Med*. 2017;77:1142–1150. doi: 10.1002/mrm.26201
18. Gotoh K, Okada T, Miki Y, Ikedo M, Ninomiya A, Kamae T, Togashi K. Visualization of the lenticulostriate artery with flow-sensitive black-blood acquisition in comparison with time-of-flight MR angiography. *J Magn Reson Imaging*. 2009;29:65–69. doi: 10.1002/jmri.21626
19. Marinkovic S, Gibo H, Milisavljevic M, Cetkovic M. Anatomic and clinical correlations of the lenticulostriate arteries. *Clin Anat*. 2001;14:190–195. doi: 10.1002/ca.1032
20. Bullitt E, Gerig G, Pizer SM, Lin W, Aylward SR. Measuring tortuosity of the intracerebral vasculature from MRA images. *IEEE Trans Med Imaging*. 2003;22:1163–1171. doi: 10.1109/TMI.2003.816964
21. Okuchi S, Okada T, Ihara M, Gotoh K, Kido A, Fujimoto K, Yamamoto A, Kanagaki M, Tanaka S, Takahashi R, et al. Visualization of lenticulostriate arteries by flow-sensitive black-blood MR angiography on a 1.5 T MRI system: a comparative study between subjects with and without stroke. *AJNR Am J Neuroradiol*. 2013;34:780–784. doi: 10.3174/ajnr.A3310
22. Shen M, Gao P, Zhang Q, Jing L, Yan H, Li H. Middle cerebral artery atherosclerosis and deep subcortical infarction: a 3T magnetic resonance vessel wall imaging study. *J Stroke Cerebrovasc Dis*. 2018;27:3387–3392. doi: 10.1016/j.jstrokecerebrovasdis.2018.08.013
23. Xu WH, Li ML, Niu JW, Feng F, Jin ZY, Gao S. Intracranial artery atherosclerosis and lumen dilation in cerebral small-vessel diseases: a high-resolution MRI Study. *CNS Neurosci Ther*. 2014;20:364–367. doi: 10.1111/cns.12224
24. Xu WH, Li ML, Gao S, Ni J, Zhou LX, Yao M, Peng B, Feng F, Jin ZY, Cui LY. In vivo high-resolution MR imaging of symptomatic and asymptomatic middle cerebral artery atherosclerotic stenosis. *Atherosclerosis*. 2010;212:507–511. doi: 10.1016/j.atherosclerosis.2010.06.035
25. Wu F, Zhang Q, Dong K, Duan J, Yang X, Wu Y, Zhang L, Li D, Fan Z, Yang Q. Whole-brain magnetic resonance imaging of plaque burden and lenticulostriate arteries in patients with different types of stroke. *Ther Adv Neurol Disord*. 2019;12:1756286419833295. doi: 10.1177/1756286419833295
26. Miyazawa H, Natori T, Kameda H, Sasaki M, Ohba H, Narumi S, Ito K, Sato M, Suzuki T, Tsuda K, et al. Detecting lenticulostriate artery lesions in patients with acute ischemic stroke using high-resolution MRA at 7 T. *Int J Stroke*. 2019;14:290–297. doi: 10.1177/1747493018806163

27. Del Bene A, Makin SD, Doubal FN, Inzitari D, Wardlaw JM. Variation in risk factors for recent small subcortical infarcts with infarct size, shape, and location. *Stroke*. 2013;44:3000–3006. doi: 10.1161/STROKEAHA.113.002227

28. Bamford J, Sandercock P, Jones L, Warlow C. The natural history of lacunar infarction: the Oxfordshire Community Stroke Project. *Stroke*. 1987;18:545–551. doi: 10.1161/01.str.18.3.545

29. Grochowski C, Krukow P, Jonak K, Stępniewski A, Wawrzycki K, Maciejewski R. The assessment of lenticulostriate arteries originating from middle cerebral artery using ultra high-field magnetic resonance time-of-flight angiography. *J Clin Neurosci*. 2019;68:262–265. doi: 10.1016/j.jocn.2019.07.003

30. Nowinski WL, Puspitasaari F, Volkau I, Marchenko Y, Knopp MV. Comparison of magnetic resonance angiography scans on 1.5, 3, and 7 Tesla units: a quantitative study of 3-dimensional cerebrovasculature. *J Neuroimaging*. 2013;23:86–95. doi: 10.1111/j.1552-6569.2011.00597.x

31. Grochowski C, Staśkiewicz G. Ultra high field TOF-MRA: a method to visualize small cerebral vessels. 7T TOF-MRA sequence parameters on different MRI scanners - Literature review. *Neurol Neurochir Pol*. 2017;51:411–418. doi: 10.1016/j.pjnns.2017.06.011

CLINICAL AND POPULATION SCIENCES